Diffusion in Brine-Saturated Reservoir Cores Studied by NMR Imaging

Stephen J. Gibbs, John J. Attard, and Laurance D. Hall
Herchel Smith Laboratory for Medicinal Chemistry, Cambridge University School of Clinical Medicine, Cambridge CB2 2PZ, United Kingdom

Characterizing fluid-solid and fluid-fluid interactions within aqueous and hydrocarbon saturated porous media remains of vital interest in hydrocarbon resource recovery (Borgia et al., 1990). Nuclear magnetic resonance (NMR) investigations of these interactions have involved studies of nuclear spin relaxation (Halperin et al., 1989; Davies et al., 1990; Davies and Packer, 1990; Kenyon et al., 1988; Kleinberg and Horsfield, 1990; Lipsicas et al., 1986) and pulsed field gradient studies (PFG) of diffusion (Packer and Zelaya, 1989). NMR imaging (QNMRI) (Attard et al., 1991a) techniques have produced spatially resolved images of nuclear spin relaxation within fluid saturated porous media (Osment et al., 1990; Rothwell and Vinegar, 1985; Attard et al., 1991b) and spatially resolved studies of spin density during fluid migration in porous media. These latter have included observations of liquid ingress into dry material (Blackband and Mansfield, 1986), liquid multiphase flow (Mandava et al., 1990; Chen et al., 1988) and particle transport (Fordham et al., 1991a).

Spatially resolved studies of fluid intradiffusion via a combination of PFG and imaging NMR techniques are especially attractive for obtaining information about local pore structure and connectivity within porous media (Callaghan et al., 1990; Callaghan et al., 1991). Although PFG NMR imging has been used in medical and botanical studies for several years (Le Bihan and Turner, 1991; Moseley et al., 1990; Merbolt et al., 1987), quantitative intradiffusion coefficient maps are relatively scarce (Merbolt et al., 1987; Callaghan and Xia, 1991).

Pulsed field gradient NMR is a well developed tool for studying molecular diffusion (Stilbs, 1987; Kärger et al., 1987). It is sensitive to the mean-square molecular displacement d^2 projected along a common direction over a time interval Δ typically on the order of 10 to 100 ms. For a homogeneous system, these values can then be related to the intradiffusion coefficient for the molecular species observed by $\mathfrak{D} = d^2/2\Delta$. For a heterogeneous system, the situation is much more complex, and the effective diffusion coefficient as defined above may be a function of both spatial position within the structure of interest and the time allowed for molecular redistribution to take place, Δ. Further, the apparent diffusion coefficient measured by a PFG NMR experiment may, for a heterogeneous system, be a function of the length scale of motion to which the experiment is sensitive. These dependencies may then allow inference of details of the structure of the heterogeneous system of interest (Callaghan et al., 1990; Callaghan et al., 1991; Tanner, 1983).

We report here an application of a PFG NMR imaging experiment for the determination of local water effective intradiffusion coefficients in two brine saturated reservoir cores. These preliminary experiments, performed with conventional NMR imaging hardware, are intended to *show the potential of this technique for obtaining information about local pore-size variations in reservoir cores via knowledge of the local restrictions to diffusion*. We believe that the results reported here are the first spatially resolved measurements of fluid intradiffusion coefficients within actual rock cores.

Experimental Methods

Pulsed field gradient NMR imaging

The NMR imaging protocol used for obtaining quantitative intradiffusion coefficient maps, LED PFG NMR imaging, has been described in detail elsewhere (Gibbs and Johnson, 1991; Gibbs et al., 1992), but for convenience we summarize important features here. A schematic of the LED PGF NMR imaging experiment employed is shown in Figure 1. The experiment is essentially an enhancement of the stimulated echo PFG experiment (Tanner, 1970), which has been shown to produce reliable results even with unshielded gradient sets (Gibbs and Johnson, 1991; Gibbs et al., 1992). It differs from the standard stimulated echo PFG NMR experiment in three respects: a train of identical magnetic field gradient pulses is applied prior to any radio-frequency excitation in order to allow transient magnetic field disturbances following a gradient pulse to achieve a pseudo-steady state; the stimulated echo is not acquired as it forms but rather is stored as longitudinal magnetization for a period T_e long enough for transient magnetic field disturbances following the final magnetic field gradient pulse to decay to a level acceptable for undistorted signal

Correspondence concerning this work should be addressed to L. D. Hall.

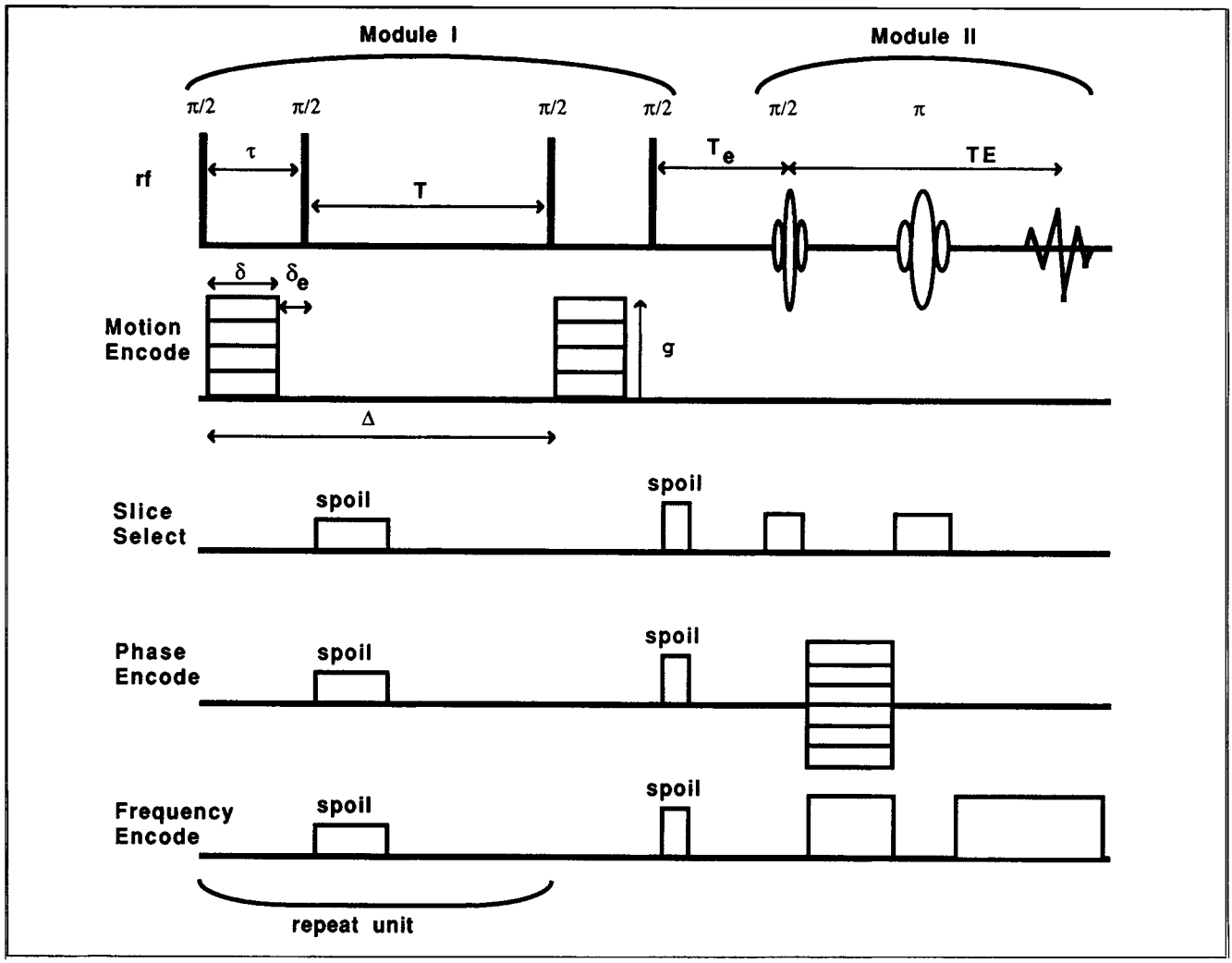

Figure 1. LED PFG imaging sequence with two modules: (I) motion sensitization; (II) imaging.

The diagram shows the sequence of events on the ratio-frequency (rf) and magnetic field gradient channels.

acquisition; an imaging module is appended to the sequence in order to provide spatial resolution of the prepared signals.

Thus, the experiment shown in Figure 1 may be considered as consisting of two separate modules. The first module serves to encode into the local magnetization information about local diffusive motion in the time interval Δ between the leading edges of two large magnetic field gradient pulses. Specifically, the local longitudinal magnetization A is related to the local, apparent intradiffusion coefficient $\mathfrak{D}$ in the direction of the applied magnetic field gradient $\vec{g}$ and the experimental parameters by (Stejskal and Tanner, 1965)

$$\frac{A}{A_0} \approx \exp[-K^2(\Delta - \delta/3)\mathfrak{D}] \tag{1}$$

where

$$A_0 \approx \frac{M_0}{2} \exp\left(\frac{-2\tau}{T_2}\right) \exp\left(\frac{-T-T_e}{T_1}\right) \tag{2}$$

$K^2 = \gamma(\int_0^\tau \vec{g}(t)dt)^2$, M_0 is the local equilibrium magnetization, T_2 is a local transverse relaxation time, and T_1 is the local longitudinal relaxation time. Other timing parameters are defined in Figure 1.

Equation 1 is only valid for homogeneous media, but deviations from this simple behavior can be small for small K^2 and heterogeneous media. More rigorous formalisms for porous media have recently been developed (Callaghan et al., 1990; Mitra and Sen, 1992). However, for the signal-to-noise ratios characteristic of data from imaging experiments, a more sophisticated analysis is probably not warranted. Note that we have neglected cross terms (Stejskal and Tanner, 1965) between the local static field gradient $\vec{g}_0$ and the pulsed gradient $\vec{g}$ and have lumped into an effective T_2 any signal loss due to diffusion in the nonuniform static magnetic field together with intrinsic spin-spin relaxation. The neglect of cross terms may not be justified for the large static magnetic field gradients in the pore spaces of rocks, but is a reasonable starting point in the absence of detailed information concerning the geometry of pore spaces and the spatial variation of magnetic susceptibility within the specimen of interest. This important point will be addressed further below. Further, note that Eq. 1 is only strictly correct for square gradient pulses.

The second module is the imaging module, and is based on the spin-warp (Edelstein et al., 1980) imaging sequence. The technique relies upon acquiring signal from selected spins from a chosen slice by a combination of frequency and phase encode gradients applied during a spin-echo experiment. This acquisition process thus causes additional T_2 modulation of A_0 during the period TE decreasing A_0 by a factor of $\exp(-TE/T_2)$.

The spatially resolved measurements, estimates of local intradiffusion coefficients, are then obtained by fitting Eq. 2 to a set of measurements of A made with different values of K^2 with $\mathfrak{D}$ and A_0 as parameters.

Experimental equipment and conditions

Experiments were performed at 2T with an Oxford Research Systems BIOSPEC1 imaging console coupled to an Oxford Instruments 31 cm, horizontal bore superconducting magnet. Custom built, balanced, sine-space, bird-cage radio-frequency coils (Bolinger et al., 1989) were used in conjunction with either a 10 cm or 20 cm ID Hemholtz-Golay, custom-built gradient set driven by pairs of Crown (model 7560) audio amplifiers. The approximate maximum gradient strengths for the two gradient sets employed are 28 and 4 G/cm, respectively.

The rock cores chosen for study are a sandstone core and a limestone core of approximately 40 mm in diameter and 70 mm in length, and 20% porosity. The sandstone core has a prominent shale band feature. The permeability of the sandstone core is in excess of 1 D and that of limestone is approximately 500 mD. Both cores were cleaned, saturated with 3% brine, and wrapped in polyvinylchloride film to help prevent evaporation and drainage of brine during the experiments. Whole core proton NMR relaxation studies of the two brine saturated cores yielded the following results. For the sandstone core, saturation-recovery data are well modeled by two components with T_1's of 540 ms (85.4%) and 81 ms (14.6%), and data obtained with a Carr-Purcell-Meiboom-Gill (CPMG) (Carr and Purcell, 1954) experiment with a refocusing pulse interval of 4.8 ms are well fit by two components with T_2's of 76 ms (64.1%) and 17 ms (35.9%); for the limestone core, saturation-recovery data are well fit by two components with T_1's of 1,557 ms (69.6%) and 223 ms (30.4%), and CPMG data with a refocusing pulse interval of 4 ms are well fit by three components with T_2's of 1,003 ms (29.9%), 234 ms (39.7%), and 44 ms (30.4%).

The experimental parameters used for diffusion imaging of the two cores are as follows: for the sandstone core, $\tau = 3.5$ ms, $T = 35$ ms, $T_e = 55$ ms, $\delta = 3$ ms, $\delta_e = 500$ μs, $TE = 5.6$ ms, and $|g| = 1.6$–23.0 G/cm, and a repetition delay between successive scans of 1.2 s; and for the limestone core, $\tau = 9$ ms, $T = 160$ ms, $T_e = 207$ ms, $\delta = 8$ ms, $\delta_e = 1$ ms, $TE = 5.2$ ms, and $|g| = 0.23$–3.76 G/cm, and a repetition delay between successive scans of 2.48 s. For both cores, 32 transients were acquired for each value of $|g|$, and hence imaging times were 1.5 and 3.0 h for each value of $|g|$ for the sandstone and limestone cores, respectively. For the sandstone core 11 values of $|g|$ were used, and for the limestone 12 values were used. The comparatively long relaxation times exhibited by the limestone core allow long evolution times to be used in the PFG experiment without dramatically sacrificing the signal-to-noise ratio of the resulting images. For this reason, it was convenient to perform the limestone experiments with our standard 20 cm diameter gradient set. The sandstone core required the use of shorter transverse evolution times τ and thus stronger gradients in order to obtain similar echo amplitude attenuations. It was therefore necessary to perform the sandstone experiments with the smaller 10 cm diameter gradient set.

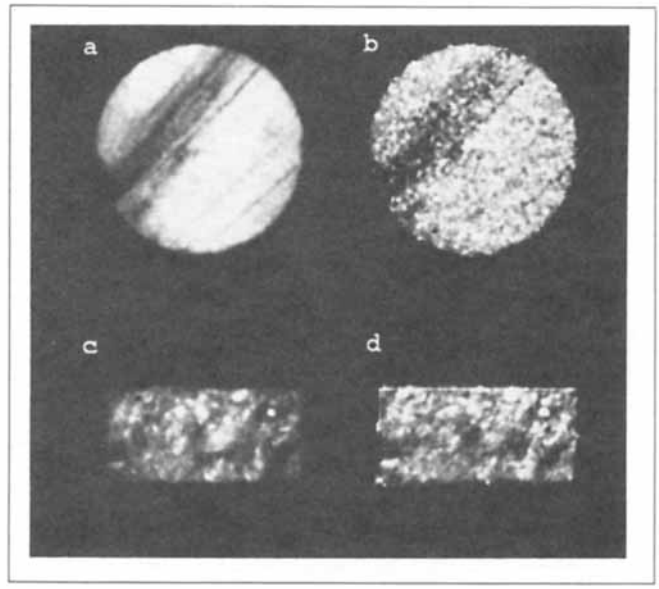

Figure 2. Spatial maps of signal intensity A_0 and diffusion coefficient $\mathfrak{D}$ for the sandstone (a) A_0 and (b) $\mathfrak{D}$ and for the limestone (c) A_0 and (d) $\mathfrak{D}$.

These maps were obtained by fitting imaging data with a model described by Eqs. 1 and 2 using a Levenburg-Marquardt least-squares minimization algorithm.

The image slice thicknesses for both the sandstone and limestone cores were 8 mm. The slice-selective radio frequency pulses used in the imaging module of the experiment were the prefocused pulses described by Fordham et al. (1991b), which yield excellent slice profiles.

The motion encoding gradient pulses were applied in the same direction as the slice select gradient for the sandstone core and as the read gradient for the limestone core. For both experiments, data were acquired in order of increasing K^2. This detail is important since, despite the precautions taken, brine still drained from the cores over the time-scale of the experiment. This effect was not precisely quantified, but was examined by repeating the acquisition for fixed values of the motion encoding gradient. This check was performed for the limestone core, for which drainage was likely to be the most pronounced because of the presence of large pores. Two images for the lowest value of K^2 were acquired, one at the beginning of the experiment and one at the end. Comparison of the two images revealed that areas corresponding to bright regions near the core surface in the images had lost signal intensity by as much as 30% over the course of the experiment but that signal loss in other regions was much less.

Figure 2 shows the derived 128×128 pixel intradiffusion coefficient and A_0 maps for the sandstone and limestone reservoir cores. Data regression onto Eq. 1 was performed with a Levenburg-Marquardt algorithm (Press et al., 1988). The applicability of Eq. 1 for describing the experimental data is demonstrated in Figure 3, which shows plots of $\ln(A/A_0)$,

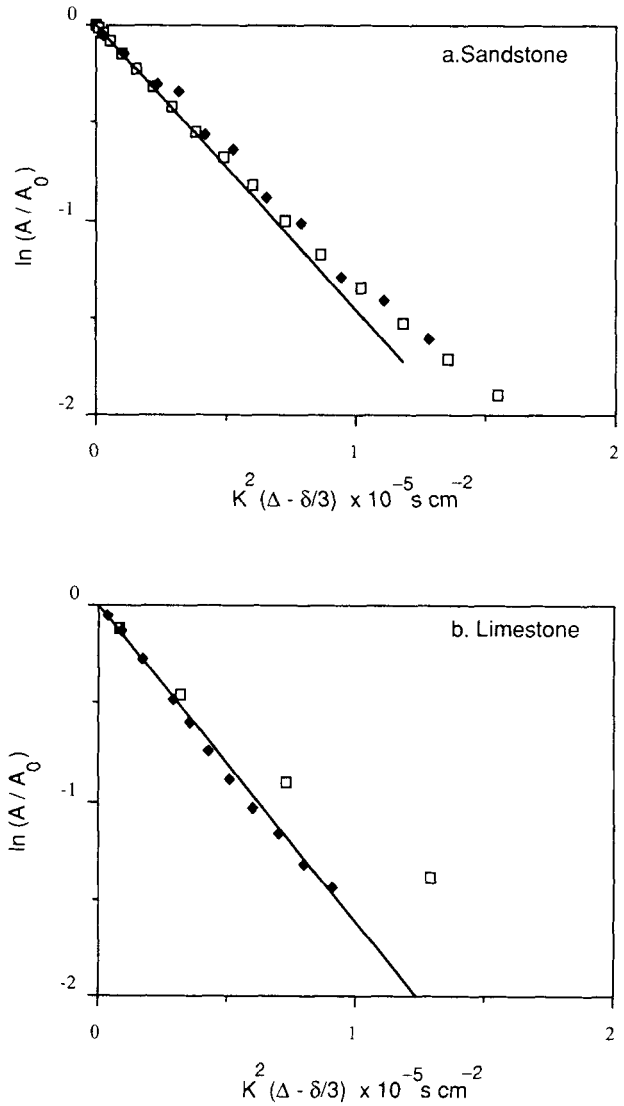

Figure 3. Whole core and slice LED PFG data.

The points represent experimental data for whole core (□), and slice (◆) experiments, and the lines indicate the slopes of $\ln(A/A_0)$ vs. $K^2(\Delta - \delta/3)$ the slice data.

integrated over the imaging slices, as a function of K^2; for both core samples, $\ln(A/A_0)$ is approximately linear in K^2.

In both sets of images in Figure 2, the contrast scales are set so that bright regions represent large A_0 or $\mathfrak{D}$. Note that there is a good correlation between large A_0 and large $\mathfrak{D}$ in both sets of images; however, there are exceptions to this correlation. Contrast in the A_0 images is a complex function of local values of T_1, T_2 and M_0, and hence it is difficult to make definitive interpretations. A particularly plausible explanation of the observed contrast is that bright regions in the A_0 images correspond primarily to areas of large pore size and hence large effective T_2 and $\mathfrak{D}$. Exceptions to this generality might be explained by spatial variations in the local porosity. This situation could be somewhat clarified by performing the experiment for several values of τ and T.

A more quantitative view of the diffusion maps is shown in Figure 4 which shows histograms for the two maps. For the

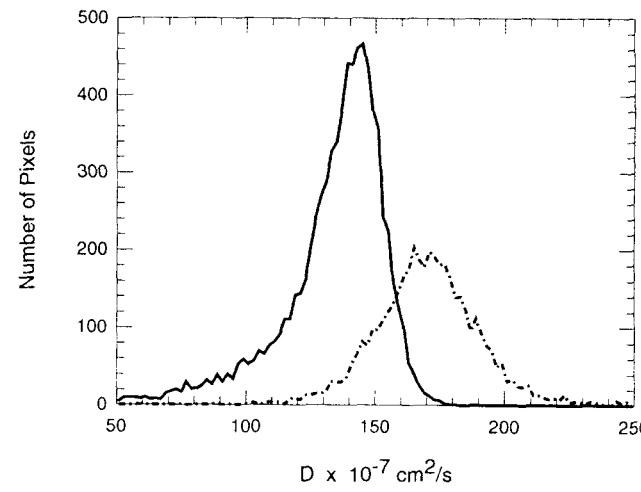

Figure 4. Distribution of pixel $\mathfrak{D}$ values for the sandstone (—) and limestone (----) cores.

The number of pixels exhibiting $\mathfrak{D}$ values in a particular range is plotted against that range.

21°C temperature at which these measurements were made, the self-diffusion coefficient of water is approximately 2.1×10^{-5} cm^2/s (Longsworth, 1960). Note that the mean values of both histograms fall well below this value presumably because of restrictions to diffusion imposed by the pore structure of the rock cores. With increasing diffusion time $\Delta = T + \tau$ one would expect the apparent diffusion coefficient to decrease as a result of these restrictions. For the values of Δ used here, the root-mean-square displacements for unrestricted diffusion of water would be approximately 9 and 18 μm for the sandstone and limestone experiments, respectively. The pixel-mean effective diffusion coefficients, $\mathfrak{D} = 1/n(\Sigma_{i=1}^{n}\mathfrak{D}_i)$, where the subscript i refers to the value at a given pixel, for the sandstone and limestone cores are 1.36×10^{-5} cm^2/s and 1.72×10^{-5} cm^2/s. Hence, average pore sizes in the sandstone core are less than 9 μm, whereas those in the limestone core are likely closer to 18 μm. These estimates could be improved by performing experiments for several different values of the diffusion time Δ.

In addition, the limestone core yields a symmetric distribution of pixel diffusion coefficients, but the sandstone core exhibits a distinctly asymmetric distribution. Similar effects have been observed for T_1 values (Attard et al., 1991b) and have been attributed to the presence of the shale band in the sandstone core. Values of the apparent diffusion coefficient in the shale-band region are approximately half of that in the rest of the core. Nevertheless, the mean, A_0 weighted, diffusion coefficients, given by $\mathfrak{D}_A = \Sigma_{i=1}^{n} A_{0,i}\mathfrak{D}_i / \Sigma_{i=1}^{n} A_{0,i}$ where the subscript i refers to a value at a given pixel i, have values of 1.40×10^{-5} cm^2/s and 1.76×10^{-5} cm^2/s for the sandstone and limestone cores respectively and thus are not significantly different from the pixel-mean diffusion coefficients for the two cores.

For both of these rock cores, whole core measurements of $\mathfrak{D}$ were also performed. The results are shown in Figure 3, which shows plots of A/A_0 as a function of K^2 for both the whole-core data and for the imaging data integrated over the slices. These whole core data were obtained with identical experimental conditions to those used for the imaging experiments except that the slice selective $\pi/2$ and π pulses were

replaced by broadband pulses and that the imaging gradients were omitted. These experiments thus provide an interesting comparison with the imaging data. Shown also in Figure 3 are lines representative of fits of Eq. 1 to the whole slice data. These lines correspond to diffusion coefficients of 1.66×10^{-5} cm^2/s for the limestone and 1.3×10^{-5} cm^2/s for the sandstone and thus agree well with the A_0 weighted mean diffusion coefficients determined from analysis of the individual pixel data. Data for the whole-core experiments and slice experiments agree well for the sandstone but not for the limestone. The deviation of the whole core data from the slice data at large K^2 may be a result of long distance scale spatial heterogeneities in the limestone core. Note, however, that the initial slopes of $\ln(A/A_0)$ vs. $K^2(\Delta - \delta/3)$ are not significantly different for the whole-core and slice data.

Conclusions

We have demonstrated the feasibility of PFG NMR imaging of local water intradiffusion coefficients within reservoir cores. Clearly, significant optimization of equipment and experimental protocol will allow improvement in the quality of the data obtainable from such experiments and in the speed of data acquisition. Specifically, it would be desirable to be able to employ stronger motion encoding field gradients. This capability would allow the realization of the same values of K^2 as used in this study with shorter transverse evolution times τ. It is desirable for 2τ to be short in comparison with the effective T_2's in order to maximize A_0. It will probably be necessary to employ shielded gradient coils to provide such large gradients in order to minimize the transient field disturbances following the large amplitude field gradient pulses. Finally, it would probably be desirable to employ a PFG experiment of the type suggested by Cotts et al. (1989) that is insensitive to the large static magnetic field gradients that are present in porous media. This type of experiment would provide two potential benefits: first, A_0 would likely be much larger since it would not be attenuated as severely by diffusion in the static field gradients present in heterogeneous rocks; and second, cross terms between the static and pulsed field gradients would be eliminated. These improvements would allow more rapid, accurate and representative observation of the local motions present in heterogeneous samples. Implementation of the above improvements, though complex, should not only broaden the scope of materials accessible to PFG NMR imaging, but also allow more detailed inferences about the local pore structure.

Acknowledgments

The authors thank BP Research for helpful discussions. This work was supported in part by the North Atlantic Treaty Organization under a Fellowship awarded to SJG in 1990. JJA thanks BP Research for a post-doctoral Fellowship, and LDH wishes to thank Dr. Herchel Smith for a generous endowment that provided the apparatus used.

Notation

A = NMR echo amplitude
d = root mean-square displacement
$\mathfrak{D}$ = diffusion coefficient
$\vec{g}$ = pulsed magnetic field gradient
$\vec{g}_0$ = static magnetic field gradient
M_0 = equilibrium magnetization
T = experimental timing parameter
T_1 = longitudinal relaxation time for nuclear magnetization
T_2 = transverse relaxation time for nuclear magnetization
T_e = experimental timing parameter
TE = experimental timing parameter, echo time

Greek letters

Δ = time allowed for diffusion
δ = duration of magnetic field gradient pulse
τ = experimental timing parameter

Subscripts

i = referring to pixel i in an image

Literature Cited

Attard, J., L. Hall, N. Herrod, and S. Duce, "Materials Mapped with NMR," *Physics World*, **4**, 41 (1991a).
Attard, J. J., T. A. Carpenter, L. D. Hall, S. Davies, N. J. Taylor, and K. J. Packer, "Spatially Resolved T_1 Relaxation Measurements in Reservoir Cores," *Magn. Reson. Imag.*, **9**, s815 (1991b).
Blackband, S., and P. Mansfield, "Diffusion in Liquid-Solid Systems by NMR Imaging," *J. Phys. C: Solid State Phys.*, **19**, L49 (1986).
Bolinger, L., M. G. Prammer, and G. S. Leigh, "A Multiple-Frequency Coil with a Highly Uniform B_1 Field," *J. Magn. Reson.*, **81**, 162 (1989).
Borgia, G. C., R. J. S. Brown, P. Fantazzini, J. Gore, P. Mansfield, B. Maraviglia, E. Mesini, and L. Sgubini, eds., *Proceedings of the First International Meeting on Recent Advances in NMR Applications to Porous Media*, Pergamon Press, New York (1990).
Callaghan, P. T., and Y. Xia, "Velocity and Diffusion Imaging in Dynamic NMR Microscopy," *J. Magn. Reson.*, **91**, 326 (1991).
Callaghan, P. T., D. MacGowan, K. J. Packer, and F. O. Zelaya, "High Resolution q-Space Imaging in Porous Structures," *J. Magn. Reson.*, **90**, 177 (1990).
Callaghan, P. T., A. Coy, D. MacGowan, K. J. Packer, and F. O. Zelaya, "Diffraction-like Effects in NMR Diffusion Studies of Fluids in Porous Solids," *Nature*, **351**, 467 (1991).
Carr, H. Y., and E. M. Purcell, "Effects of Diffusion on Free Precession in Nuclear Magnetic Resonance Experiments," *Phys. Rev.*, **94**, 630 (1954).
Chen, J. D., M. M. Dias, S. Patz, and L. M. Schwartz, "Magnetic Resonance Imaging of Immiscible Fluid Displacement in Porous Media," *Phys. Rev. Lett.*, **61**, 1489 (1988).
Cotts, R. M., M. J. R. Hoch, T. Sun, and J. T. Marker, "Pulsed Field Gradient Stimulated Echo Methods for Improved NMR Diffusion Measurements in Heterogeneous Systems," *J. Magn. Reson.*, **83**, 252 (1989).
Davies, S., M. Z. Kalam, K. J. Packer, and F. O. Zelaya, "Pore Size Distributions from Nuclear Magnetic Resonance Spin-Lattice Relaxation Measurements of Fluid Saturated Porous Solids: II. Applications to Reservoir Core Samples," *J. Appl. Phys.*, **67**, 3170 (1990).
Davies, S., and K. J. Packer, "Pore Size Distributions from Nuclear Magnetic Resonance, Spin-Lattice Relaxation Measurements of Fluid Saturated Porous Solids: I. Theory and Simulation," *J. Appl. Phys.*, **67**, 3163 (1990).
Edelstein, W. A., J. M. S. Hutchison, G. Johnson, and T. Redpath, "Spin Warp NRM Imaging and Applications to Human Whole Body Imaging," *Phys. Med. Biol.*, **25**, 771 (1980).
Fordham, E. J., T. P. L. Roberts, T. A. Carpenter, L. D. Hall, and C. Hall, "Dynamic NMR Imaging of Rapid Depth Filtration of Clay in Porous Media," *AIChE J.*, **37**(12), 1900 (1991a).
Fordham, E. J., T. P. L. Roberts, T. A. Carpenter, L. D. Hall, G. C. Maitland, and C. Hall, "Nuclear Magnetic Resonance Imaging of Simulated Voids in Cement Slurries," *AIChE J.*, **37**(12), 1895 (1991b).
Gibbs, S. J., and C. S. Johnson, Jr., "A PFG NMR Experiment for Accurate Diffusion and Flow Studies in the Presence of Eddy Currents," *J. Magn. Reson.*, **93**, 395 (1991).
Gibbs, S. J., T. A. Carpenter, and L. D. Hall, "Diffusion Imaging with Unshielded Gradients," in press, *J. Magn. Reson.* (1992).

Halperin, W. P., F. D'Orazio, S. Bjattacharja, and J. C. Tarczon, "Molecular Dynamics in Restricted Geometries," J. Klafter and J. M. Drake, eds.. Wiley, New York, p. 311 (1989).
Karger, J., H. Pfeifer, and W. Heink, *Advances in Magnetic Resonance*, J. S. Waugh, ed., Vol. 12, p. 1, Academic Press, San Diego (1988).
Kenyon, W. E., P. I. Day, C. Straley, and J. F. Willemsen, "Compact and Consistent Representation of Rock NMR Data for Permeability Estimation," SPE 15643, **3** (1986).
Kleinberg, R. L., and M. A. Horsfield, "Transverse Relaxation Processes in Sedimentary Rock," *J. Magn. Reson.*, **88**, 9 (1990).
Le Bihan, D., and R. Turner, "Single-Shot Diffusion Imaging at 2.0 T," *Magn. Reson. Med.*, **19**, 221 (1991).
Lipsicas, M., M. Banavar, and J. Willemsen, "Surface Relaxation and Pore Sizes in Rocks—A Nuclear Magnetic Resonance Analysis," *Appl. Phys. Lett.*, **48**, 1544 (1986).
Longsworth, L. G., "The Mutual Diffusion of Light and Heavy Water," *J. Phys. Chem.*, **64**, 914 (1960).
Osment, P. A., K. J. Packer, M. J. Taylor, J. J. Attard, T. A. Carpenter, L. D. Hall, N. J. Herrod, and S. J. Doran, "NMR Imaging of Fluids in Porous Solids," *Phil. Trans. Roy. Soc. Lond. A*, **333**, 441 (1990).
Mandava, S. S., A. T. Watson, and C. M. Edwards, "NMR Imaging of Saturation During Immiscible Displacements," *AIChE J.*, **36**, 1680 (1990).
Merbolt, K. D., W. Hanicke, and J. Frahm, "NRM Imaging of Restricted Diffusion," *Ber. Bunsenges. Phys. Chem.*, **91**, 1124 (1987).
Mitra, P. P., and P. N. Sen, "Effects of Microgeometry and Surface Relaxation on NMR Pulsed-Field-Gradient Experiments: Simple Pore Geometries," *Phys. Rev. B*, **45**, 143 (1992).
Moseley, M. E., Y. Cohen, J. Kucharczyk, J. Mintorovitch, H. S. Asgari, M. F. Wendland, J. Tsuruda, and D. Norman, "Diffusion-Weighted MR Imaging of Anisotropic Water Diffusion in Cat Central Nervous System," *Radiology*, **176**, 439 (1990).
Packer, K. J., and F. O. Zelaya, "Observations of Diffusion of Fluids in Porous Solids by Pulsed Field Gradient NMR," *Coll. and Surf.*, **36**, 221 (1989).
Press, W. H., S. A. Flannery, S. A. Teukolsky, and W. T. Vetterling, *Numerical Recipes in C: The Art of Scientific Computing*, Cambridge University Press, New York (1988).
Rothwell, W. P., and H. J. Vinegar, "Petrophysical Applications of NMR Imaging," *Appl. Opt.*, **24**, 3969 (1985).
Stejskal, E. O., and J. E. Tanner, "Spin Diffusion Measurements: Spin Echoes in the Presence of a Time-Dependent Field Gradient," *J. Chem. Phys.*, **42**, 282 (1965).
Stilbs, P., "Fourier Transform Pulsed-Gradient Spin-Echo Studies of Molecular Diffusion," *Prog. NMR Spectrosc.*, **19**, 1 (1987).
Tanner, J. E., "Use of the Stimulated Echo in NMR Diffusion Studies," *J. Chem. Phys.*, **52**, 2523 (1970).
Tanner, J. E., "Intracellular Diffusion of Water," *Arch. Biochem. Biophys.*, **224**, 416 (1983).

Manuscript received Mar. 17, 1992, and revision received Oct. 5, 1992.